Topographic advection on fault-bend folds: Inheritance of valley positions and the formation of wind gaps

Scott R. Miller*
Rudy L. Slingerland   Department of Geosciences, Pennsylvania State University, University Park, Pennsylvania 16802, USA

ABSTRACT

Drainage basins formed along the flanks of any individual linear mountain range or fault block are commonly observed to be self-similar in planform, uniformly spaced, and in some cases aligned with drainage basins on the opposing flank. Data from the Siwalik Hills, Nepal, illustrate this organization where drainage basins and valleys are aligned across the main divide. We suggest that valley alignment is a consequence of advection of topography across the divide. To explore this hypothesis, numerical experiments were conducted using a landscape evolution model of a fault-bend fold that simulates detachment-limited stream incision and linear hillslope diffusion. Results show that the presence of incised valleys and a lateral component of bedrock motion are necessary and sufficient conditions for advection of relief across the divide, a mechanism by which wind gaps form and valley spacing on the far side of a ridge is inherited from that on the near side. This topographic inheritance is promoted by low rock erodibility, low precipitation rates, fast bedrock velocities, and/or intermediate fault dips.

Keywords: geomorphology, Siwalik Hills, fluvial erosion, landscape evolution, models.

INTRODUCTION

Since Playfair (1802) demonstrated that streams generally form their own valleys, scientists have wondered what factors determine valley pattern, especially density, orientation, and spacing. Along mountain ranges and fault-bounded ridges, valleys (or drainage basins) are commonly oriented transversely and spaced regularly in proportion to the range half-width (Hovius, 1996; Talling et al., 1997), consistent with other observations of drainage basin self-similarity (Rodriguez-Iturbe and Rinaldo, 1997). Although we now have a good understanding of what determines drainage and valley density (e.g., Tucker and Bras, 1998), the controls on the exact locations of valleys remain poorly understood.

A particularly curious phenomenon of linear mountain ranges and fault blocks is the common alignment of valleys across their main drainage divides (Fig. 1). These valleys often terminate headward at saddles in the ridge crest. Horton (1945) attributed such saddles to competitive erosion between two adjacent drainage basins, but this mechanism does not explain the strong alignment of valleys on opposite sides of the ridge shown in Figure 1. We might expect linear erodible zones such as faults or fracture zones to enhance alignment and saddle development, as has been argued for the western flank of the Southern Alps (Norris et al., 1990). However, transverse valley spacing varies over nearly three orders of magnitude as a linear function of mountain range half-width (Hovius, 1996;

Talling et al., 1997), and such a relationship also would have to exist for transverse structures to explain the observations. While fracture density theoretically influences erosion mechanisms (Whipple et al., 2000) and locally affects stream directions and locations (e.g., Ericson et al., 2005), we are not aware of a theory for why fracture density should be regularly spaced as a function of range half-width.

Here we propose an alternative explanation for these systematic patterns of stream valleys on opposing sides of active contractional mountain ranges: they emerge through self-organization of drainage basins responding to spatially nonuniform lateral advection of rock mass (relief) common in such systems. A horizontal component of bedrock motion is the norm rather than the exception in active convergent orogens, at the scales of individual structures and of entire mountain belts, and has been shown to influence the large-scale steady-state geomorphology of such orogens (Adams, 1985; Koons, 1990; Willett et al., 2001). While topography has been conjectured to advect laterally with bedrock (Koons, 1995; Willett et al., 2001), the consequences of this remain untested. We show that in the Siwalik Hills of Nepal and in a numerical landscape evolution model of a fault-bend fold, where both topography and bedrock move along the bedrock streamlines, topographic relief created at proximal sites, relative to the source of advection, influences the positions of valleys and ridges at distal sites, even across the drainage divide. Valleys are advected up the backlimb and beheaded at the divide to form wind gaps. Some valley and ridge topography is then advected to the distal ridge flank, transferring with it characteristics such as valley spacing.

EMPIRICAL DATA

The Siwalik Hills of Nepal are a series of linear ridges that exhibit relatively uniformly spaced, transversely oriented valleys that are locally aligned across the main ridge line (Fig. 1). They have formed over active fault-bend folds on the Main Frontal thrust and Main Dun thrust, and are thus the southernmost topographic expressions of active deformation
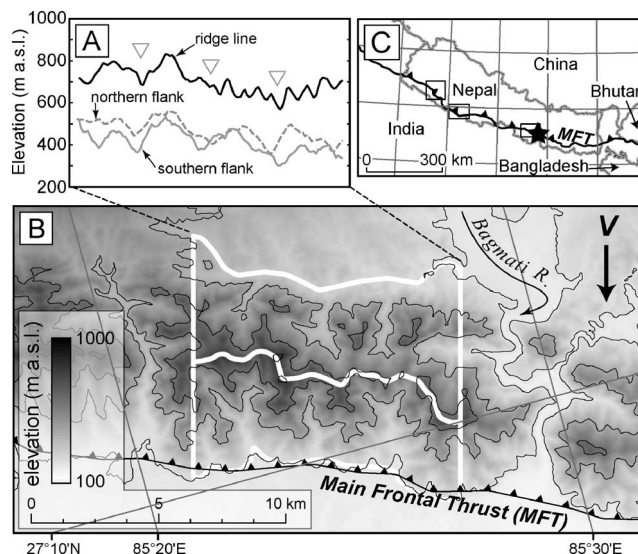
Figure 1. A: Profiles of ridge line and mean elevations from northern and southern ridge flanks along segment of Siwalik Hills near Bagmati River. Mean elevations and ridge crest elevations covary visually (a.s.l.—above sea level). Triangles indicate prominent saddles between aligned valleys. B: Topographic map showing regions averaged (marked in white) in direction of hanging-wall slip (V) to produce profiles above. Contour interval is 200 m. C: Location map of B (star) and other areas analyzed in this study (boxes).

within the Himalayan orogen. Hanging-wall deformation of Miocene–Pleistocene siltstones, sandstones, and conglomerates of the Siwalik Group is consistent with kinematic models of fault-bend folds (Lavé and Avouac, 2000). Average ramp dips (α) beneath the Siwalik Hills range from 30° to 45°, although ramps reach local maxima of ~60°. Hanging-wall thicknesses (T) range from 4 to 6 km (Mugnier et al., 1999; Lavé and Avouac, 2000). Fault slip rates (V) measured over Holocene time scales are 0.04–0.21 mm/yr (Lavé and Avouac, 2000; Mugnier et al., 2004). Erosional fluxes on these ridges have equaled tectonic fluxes over the Quaternary, indicating the achievement of flux and approximate topographic steady states (Hurtrez et al., 1999).

We cross-correlated mean elevations of opposing ridge flanks at 10 locations along the Siwalik Hills in order to characterize the relation between valley locations across the ridge line (GSA Data Repository Appendix DR1[1]). As shown in the example in Figure 1, approximately strike-parallel topographic profiles of mean elevation were calculated for each side of a given ridge segment, averaged between ridge crest and mountain front, using 3-arc-second Shuttle Radar Topography Mission (SRTM) digital elevation models. Segments were chosen along linear sections of the ridge and between water gaps. Elevations of each ridge flank were averaged in the direction of advection, or parallel to hanging-wall slip, in order to determine whether topographic characteristics are transferred in this direction. This direction was approximated as perpendicular to the small circle drawn through the Himalayan arc (Bilham et al., 1997), which is consistent at our sites with global positioning system data (Bilham et al., 1997), seismic moment tensor solutions (Pandey et al., 1995), and slickenlines on individual faults (Mugnier et al., 1999). A simple linear cross-correlation was performed between mean elevation vectors for the distal and proximal ridge flanks of each segment, yielding a Pearson product-moment correlation coefficient, r, which ranges from −0.18 to 0.89 with a median of 0.28 (Table DR1; see footnote 1). A consideration of model results will allow us to better assess the significance of these correlations.

MODEL DESCRIPTION

To determine the expected cross-correlation of steady-state topography across Siwalik-type ridge crests, we used a landscape evolution model that predicts landscape elevation, h, as a function of horizontal locations, x and y, and
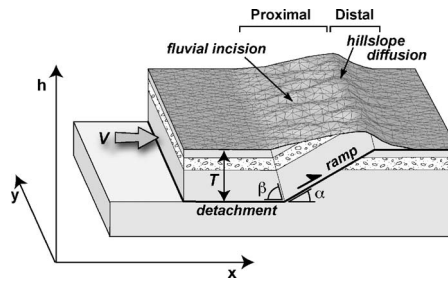
Figure 2. Schematic of kinematic fault-bend fold and landscape evolution model. Strata are shown for visual purposes and do not reflect lithology. Model topography is shown ($N_e = 5$, $D = 0$, $\alpha = 30°$; parameters and variables are defined in text).

time, t. Without much loss of generality, we can consider the case of a fault-bend fold in which a hanging wall of thickness T moves laterally above a horizontal detachment at constant speed, V, and then up a ramp with dip α (Fig. 2). The upper tip of this ramp is set to the initial elevation of the model surface, which is the local erosional base level, at which the fault bends back into a flat. Bedrock streamlines parallel the fault following a simple kinematic rule that preserves line length and conserves mass (Suppe, 1983). As bedrock passes over the ramp, also with velocity V, it is deformed in a kink band between planar axial surfaces with dips β that project from the flat-ramp-flat intersections. This rule adequately predicts deformation in many fold and thrust belts over periods greater than a single seismic cycle (e.g., Suppe, 1983; Lavé and Avouac, 2000). Model rules are defined further in Appendix DR2 (see footnote 1).

We simulate surface processes with rules for detachment-limited fluvial incision and hillslope diffusion, which represent end-member processes for topographic relief production and topographic smoothing, respectively. The rate of fluvial erosion in bedrock channels, E (ms·yr^{-1}), is assumed to be proportional to unit stream power, which has been shown to reasonably predict long-term erosion rates in tectonically active settings (e.g., Kirby and Whipple, 2001). Using common empirical relations to substitute drainage area for discharge and stream width (Appendix DR2), unit stream power can be written as

$$E = KA^{1/2}S, \quad (1)$$

where A is drainage area (m^2), S is channel slope, and K is an erosion coefficient (yr^{-1}), encompassing factors such as rock strength and precipitation rate.

Hillslope erosion is simulated with an equation for linear diffusion in two horizontal dimensions (Culling, 1965):

$$E = -\kappa\left(\frac{\partial^2 h}{\partial x^2} + \frac{\partial^2 h}{\partial y^2}\right). \quad (2)$$

where κ is a spatially constant diffusivity (m^2·yr^{-1}). Although linear diffusion may not strictly capture landsliding, which is common in active orogens, the details of hillslope sediment transport are less important for our analysis.

Combining Equations 1 and 2 with a tectonic velocity field and making use of nondimensional variables (Appendix DR3; see footnote 1) yields a continuity equation for landscape evolution:

$$\frac{\partial h^*}{\partial t^*} = \sin\alpha + \cos\alpha\frac{\partial h^*}{\partial x^*}$$
$$+ D\left(\frac{\partial^2 h^*}{\partial x^{*2}} + \frac{\partial^2 h^*}{\partial y^{*2}}\right) - N_e A^{*1/2}S, \quad (3)$$

in which $D = \kappa/TV$ and $N_e = KT/V$. The nondimensional diffusion number, D, is the inverse of the conventional Péclet number and thus describes the relative efficacy of hillslope diffusion versus bedrock velocity. Similarly, the nondimensional fluvial erosion number, N_e, describes the relative efficacy of fluvial incision versus bedrock velocity. Solutions to Equation 3 are obtained using CHILD, a finite-difference landscape evolution model that operates on an irregular grid (Tucker et al., 2001). Although computational nodes do not move their positions in x or y directions, we simulate lateral displacement of bedrock and topography at each time step by including an apparent lateral component that is interpolated from adjacent nodal elevations. As in our treatment of streams, diffusion erodes but does not explicitly deposit sediment, which is assumed to quickly enter the fluvial system and exit the model space at any of the four open boundaries. Finally, we assume steady precipitation and fault slip rates.

MODEL RESULTS

Five numerical experiments were conducted to explore parameter space (Table DR2; see footnote 1). The first experiment simulated topography subject to vertical rock uplift bounded by two vertical faults and varying N_e, D, T, and lateral boundary conditions. The remaining experiments simulated topography above a fault-bend fold for various combinations of N_e, D, and α. Consistent with landscape evolution models that include tectonic shortening (Willett et al., 2001), steady-state model topography varies between being symmetrical when erosion is effective relative to tectonic velocity (large N_e) and being asymmetrical when erosion is less effective (small N_e) (Fig. 3).
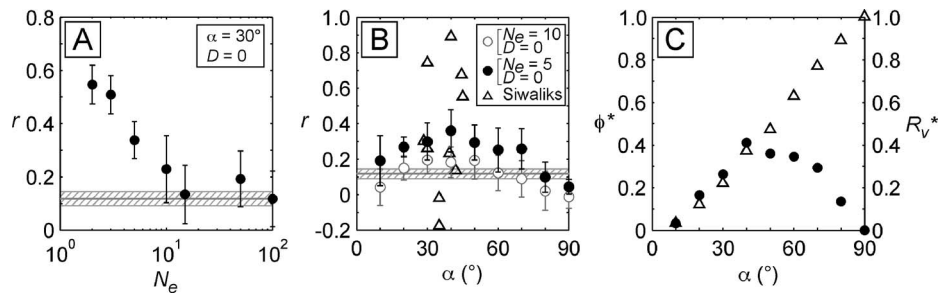
The basic analysis of model output consists of cross-correlation of mean elevations across the ridge crest in the same manner described here for the Siwalik Hills. Because simulated steady-state topography is sensitive to initial
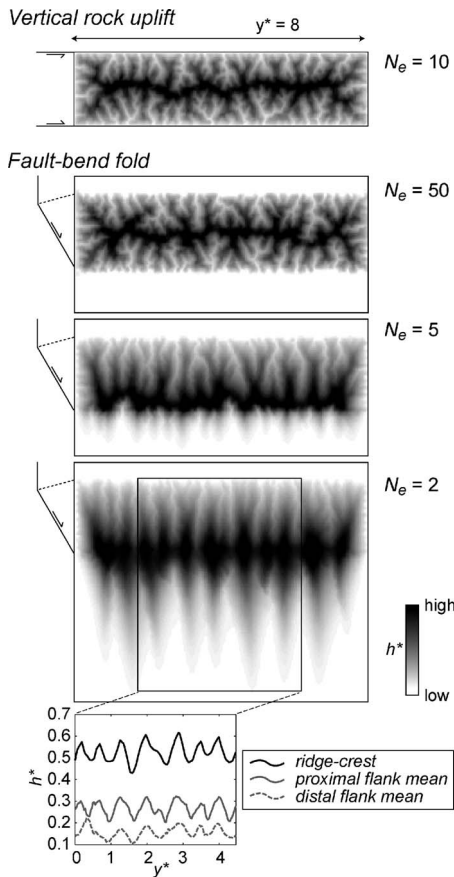
Figure 3. Maps of topography formed by model with vertical uplift and over fault-bend fold for different fluvial erosion numbers, N_e, with fixed ramp dip, $\alpha = 30°$, and diffusion number, $D = 0$. Erosion coefficient K was actual parameter varied, but corresponding changes in T or V, maintaining same N_e, generate same results. Rotated cross sections are shown at left; strike-wise topographic profiles are shown at bottom. Note that $y^* = y/T$, $x^* = x/T$, and $h^* = h/T$. See text for definitions of parameters and variables.

Figure 4. Correlation of topography across fault-bend fold ridge as measured by mean correlation coefficient, r, for various values of (A) N_e and (B) α. 95% confidence interval is shown. Null hypothesis is represented by dark black line (mean) and hachured region (95% confidence interval). C: Plot of nondimensional flux of bedrock through peaks, ϕ^* (circles), and mean nondimensional cross-valley relief, R_v^*, of proximal valleys (triangles) calculated for model topography ($N_e = 10$, $D = 0$). See text for definitions of parameters and variables.

conditions (Howard, 1994), we used a Monte Carlo approach to constrain model uncertainty (Borradaile, 2003). For each set of parameters, multiple realizations of each model ($n = 10$–200 depending on computational cost) were created using different horizontal initial surfaces of randomly perturbed node elevations.

The correlation coefficient of the vertical rock uplift model provides the null hypothesis for testing whether lateral advection increases the cross-correlation of mean elevations across a ridge crest. We argue that greater correlation coefficients are due to topographic inheritance as relief is advected from one side of the range to the other. For the specific parameters in the null hypothesis model ($N_e = 10$, $D = 0$), r has a normal distribution around a mean value of 0.12 ± 0.03 (95% confidence interval): a minor though nonzero correlation that arises even with pure rock uplift. The correlation coefficient is not statistically different at the 5%
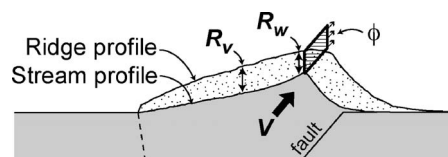
significance level for realizations with different T, N_e, or D, or for reflected lateral boundaries (Table DR2; see footnote 1). Thus, model range width, erosional parameters, and the finite length of our model domain do not influence the relative positions of drainage basins undergoing vertical uplift.

In contrast to the simulations with vertical rock uplift, the fault-bend fold model shows considerable variation in correlation coefficient. In simulations where $\alpha = 30°$ and N_e is varied, the alignment of elongate valleys is visible in map view and in profiles for low values of N_e (Fig. 3). The correlation coefficient is significantly larger than the null hypothesis at the 5% significance level for $N_e < 10$ and approaches the value of the null hypothesis as N_e increases (Fig. 4A). For a given ramp dip, low values of N_e promote advection of topography because bedrock velocities are high relative to erosion rates.

The topographic cross-correlation is relatively insensitive to diffusion in our simulations. For example, when $N_e = 10$ and $\alpha = 30°$, r varies significantly only at high values of D because diffusion dominates over fluvial incision, valleys disappear, and much of the correlation comes from edge effects as the ridge becomes mound shaped (Table DR2; see footnote 1).

Ramp dip (α) exerts a strong influence on

the cross-correlation. The correlation coefficient reaches a maximum at $\alpha \approx 45°$, which is significantly greater than the null hypothesis when $N_e < 10$ (Fig. 4B). This optimum reflects the competition between the formation of cross-valley relief (R_v) on the proximal side of the ridge, and therefore wind-gap relief (R_w) (both promoted by a steeper ramp dip), and the rate of advection (promoted by a gentler ramp dip) (Fig. 4C). To explore this idea, consider a volumetric lateral flux of peaks across the divide per unit length, ϕ (Fig. 5). This flux can be nondimensionalized as $\phi^* = (R_w/R_w^0) \cos \alpha$, where R_w^0 is mean wind-gap relief when $\alpha = 90°$ against ramp dip, ϕ^* exhibits the same behavior as r (Fig. 4C), supporting the idea that cross-correlation of elevations behaves consistently with the potential amount of local relief that crosses a ridge.

DISCUSSION AND CONCLUSIONS

Model and empirical data from the Siwalik Hills show that topography on linear ridges undergoing lateral advection may cross-correlate across ridge crests, indicating valley or drainage basin alignment. Variance in the correlation coefficient in the Siwalik Hills, from strongly positive to weakly negative (Fig. 4B), is expected because the topographic surfaces advected into their proximal flanks are not uniform and horizontal, as in the model, but spatially variable and complex. Proximal valleys might not maintain steady positions over long periods. Furthermore, the approximate values of N_e in the Siwalik Hills fall in a large range ($\sim$5–125; Appendix DR4; see footnote 1); in light of the model, these are expected to generate correlation coefficients varying from significantly positive to indistinguishable from the null hypothesis.

In the fault-bend fold models, valleys advected up the proximal side of the ridge are beheaded at the drainage divide by distal valleys, meaning that proximal drainage areas are transferred to the distal side (Bishop, 1995). Stream courses are not preserved in the transfer. Our model suggests that in the course of

Figure 5. Cross section of model topography ($N_e = 5$, $D = 0$, $\alpha = 30°$; see text for definitions of parameters and variables) showing ridge-top and valley-bottom elevation profiles. Cross-valley relief (R_v) and wind-gap relief (R_w) are, respectively, elevation differences between ridge lines (peaks) and valley bottoms (saddles) in strike direction. Striped area represents unit flux of bedrock through peaks along ridge line, ϕ (vertical exaggeration = 2).

beheading, topographic information in the form of ridge and valley locations is actually passed across the drainage divide: the beheader inherits topography from the beheaded. Distal valleys, especially close to the divide, naturally form where low topography is advected across the divide. Although bedrock streamlines are inclined upward, this valley position is transmitted to the foot of the range by further advection as well as downward erosion.

Valley beheading has been suspected in other convergent, steady-state orogens, for example at the crest of the Central Range of Taiwan (N. Hovius, 2003, personal commun.). Elsewhere, topographic advection is invoked as the cause of stream piracy or capture (Koons, 1995). For example, whole valleys and their drainage courses have been captured and thus transferred from the eastern to western flank of the Southern Alps, as inferred from geologic mapping and fish phylogeography (Waters and Wallis, 2000; Craw et al., 2003). Whereas the current study illustrates the passage of topography across drainage divides due to beheading, capture is likely promoted by similar conditions. Furthermore, our study focuses on a particular steady-state landscape, but we suggest that our predictions extend to larger convergent orogens and in a limited degree to transient landscapes, such as retreating escarpments or normal-faulted mountain ranges where traces of capture are evident and beheading is likely (e.g., Harbor, 1997).

These results also suggest that some saddles in thrust-bounded mountain ranges are probably degraded wind gaps, i.e., the beheaded remnants of fluvial valleys that have been advected to the ridge line. In contrast to wind gaps commonly observed above growing structures (e.g., Keller et al., 1999), wind gaps formed by the mechanism described here do not reflect the courses of range-crossing antecedent streams, do not contain any information on fold propagation, and may develop on landforms in steady state.

We conclude that topographic advection produces wind gaps and an alignment of elongate valleys. When wind gaps or saddles are present in a ridge crest and fault dip is <90°, some topography will be advected across the crest and influence valley locations on the distal side. Model results show that topographic advection and resulting topographic inheritance is promoted by low rock erodibility, low precipitation rates, thin hanging walls, and/or fast fault slip rates. Inheritance is also promoted by roughly equal rock uplift and lateral advection rates (fault dip ~45°): the former develops deep valleys and the latter carries them across the divide. Although drainage divides are frequently thought of as geomorphic barriers, these divides can be permeable to the flow of topographic information.

REFERENCES CITED

Adams, J., 1985, Large-scale tectonic geomorphology of the Southern Alps, New Zealand, in Morisawa, M., and Hack, J.T., eds., Tectonic geomorphology: London, Allen & Unwin, p. 105–128.

Bilham, R., Larson, K.M., Freymueller, J.T., and Project Idylhim Members, 1997, GPS measurements of present-day convergence across the Nepal Himalaya: Nature, v. 386, p. 61–64, doi: 10.1038/386061a0.

Bishop, P., 1995, Drainage rearrangement by river capture, beheading and diversion: Progress in Physical Geography, v. 19, p. 449–473.

Borradaile, G., 2003, Statistics of earth science data: Berlin, Springer-Verlag, 351 p.

Craw, D., Nelson, E., and Koons, P.O., 2003, Structure and topographic evolution of the Main Divide in the Landsborough-Hopkins area of the Southern Alps, New Zealand: New Zealand Journal of Geology and Geophysics, v. 46, p. 553–562.

Culling, W.E.H., 1965, Theory of erosion on soil-covered slopes: Journal of Geology, v. 73, p. 230–254.

Ericson, K., Migon, P., and Olvmo, M., 2005, Fractures and drainage in the granite mountainous area; a study from Sierra Nevada, USA: Geomorphology, v. 64, p. 97–116.

Harbor, D.J., 1997, Landscape evolution at the margin of the Basin and Range: Geology, v. 25, p. 1111–1114.

Horton, R.E., 1945, Erosional development of streams and their drainage basins; hydrophysical approach to quantitative morphology: Geological Society of America Bulletin, v. 56, p. 275–370.

Hovius, N., 1996, Regular spacing of drainage outlets from linear mountain belts: Basin Research, v. 8, p. 29–44.

Howard, A.D., 1994, A detachment-limited model of drainage basin evolution: Water Resources Research, v. 30, p. 2261–2285, doi: 10.1029/94WR00757.

Hurtrez, J.E., Lucazeau, F., Lavé, J., and Avouac, J.P., 1999, Investigations of the relationships between basin morphology, tectonic uplift, and denudation from study of an active fold belt in the Siwalik Hills, central Nepal: Journal of Geophysical Research, v. 104, p. 12,779–12,796, doi: 10.1029/1998JB900098.

Keller, E.A., Gurrola, L., and Tierney, T.E., 1999, Geomorphic criteria to determine direction of lateral propagation of reverse faulting and folding: Geology, v. 27, p. 515–518, doi: 10.1130/0091-7613(1999)027<0515:GCTDDO>2.3.CO;2.

Kirby, E., and Whipple, K., 2001, Quantifying differential rock-uplift rates via stream profile analysis: Geology, v. 29, p. 415–418, doi: 10.1130/0091-7613(2001)029<0415:QDRURV>2.0.CO;2.

Koons, P.O., 1990, Two-sided orogen; collision and erosion from the sandbox to the Southern Alps, New Zealand: Geology, v. 18, p. 679–682, doi: 10.1130/0091-7613(1990)018<0679:TSOCAE>2.3.CO;2.

Koons, P.O., 1995, Modeling the topographic evolution of collisional belts: Annual Review of Earth and Planetary Sciences, v. 23, p. 375–408, doi: 10.1146/annurev.ea.23.050195.002111.

Lavé, J., and Avouac, J.P., 2000, Active folding of fluvial terraces across the Siwaliks Hills, Himalayas of central Nepal: Journal of Geophysical Research, v. 105, p. 5735–5770, doi: 10.1029/1999JB900292.

Mugnier, J.L., Leturmy, P., Mascle, G., Huyghe, P., Husson, L., Chalaron, E., Vidal, G., and Delcaillau, B., 1999, The Siwaliks of western Nepal; I, Geometry and kinematics: Journal of Asian Earth Sciences, v. 17, p. 629–642, doi: 10.1016/S1367-9120(99)00038-3.

Mugnier, J.L., Huyghe, P., Leturmy, P., and Jouanne, F., 2004, Episodicity and rates of thrust-sheet motion in the Himalayas (western Nepal), in McClay, K.R., ed., Thrust tectonics and hydrocarbon systems: Tulsa, Oklahoma, American Association of Petroleum Geologists, p. 91–114.

Norris, R.J., Koons, P.O., and Cooper, A.F., 1990, The obliquely-convergent plate boundary in the South Island of New Zealand; implications for ancient collision zones: Journal of Structural Geology, v. 12, p. 715–725, doi: 10.1016/0191-8141(90)90084-C.

Pandey, M.R., Tandukar, R.P., Avouac, J.P., Lavé, J., and Massot, J.P., 1995, Interseismic strain accumulation on the Himalayan crustal ramp (Nepal): Geophysical Research Letters, v. 22, p. 751–754, doi: 10.1029/94GL02971.

Playfair, J., 1802, Illustrations of the Huttonian theory of the Earth: New York, Dover, 528 p.

Rodriguez-Iturbe, I., and Rinaldo, A., 1997, Fractal river basins; chance and self-organization: Cambridge, Cambridge University Press, 547 p.

Suppe, J., 1983, Geometry and kinematics of fault-bend folding: American Journal of Science, v. 283, p. 684–721.

Talling, P.J., Stewart, M.D., Stark, C.P., Gupta, S., and Vincent, S.J., 1997, Regular spacing of drainage outlets from linear fault blocks: Basin Research, v. 9, p. 275–302, doi: 10.1046/j.1365-2117.1997.00048.x.

Tucker, G.E., and Bras, R.L., 1998, Hillslope processes, drainage density, and landscape morphology: Water Resources Research, v. 34, p. 2751–2764, doi: 10.1029/98WR01474.

Tucker, G.E., Lancaster, S.T., Gasparini, N.M., Bras, R.L., and Rybarczyk, S.M., 2001, An object-oriented framework for distributed hydrologic and geomorphic modeling using triangulated irregular networks: Computers & Geosciences, v. 27, p. 959–973, doi: 10.1016/S0098-3004(00)00134-5.

Waters, J.M., and Wallis, G.P., 2000, Across the Southern Alps by river capture? Freshwater fish phylogeography in South Island, New Zealand: Molecular Ecology, v. 9, p. 1577–1582, doi: 10.1046/j.1365-294x.2000.01035.x.

Whipple, K.X, Hancock, G.S., and Anderson, R.S., 2000, River incision into bedrock; mechanics and relative efficacy of plucking, abrasion, and cavitation: Geological Society of America Bulletin, v. 112, p. 490–503, doi: 10.1130/0016-7606(2000)112<0490:RIIBMA>2.3.CO;2.

Willett, S.D., Slingerland, R., and Hovius, N., 2001, Uplift, shortening, and steady state topography in active mountain belts: American Journal of Science, v. 301, p. 455–485.

*Topographic advection on fault-bend folds: Inheritance of valley positions and the
formation of wind gaps*

S.R. Miller and R.L. Slingerland
Department of Geosciences, Pennsylvania State University, University Park,
Pennsylvania 16802, USA; email: srmiller@geosc.psu.edu

APPENDIX DR1. Topographic cross-correlation

Swath topographic profiles of mean elevation measured the length of ridge flanks—either the proximal or distal side as defined in the paper—demarcate the general positions of transversely oriented valleys and interfluves along linear ridge segments. For this, we used 3 arc-second SRTM digital elevation models projected into the local UTM projection and resampled at a 90 m resolution. Swath profiles were produced by averaging elevation data sampled parallel to the direction of hanging-wall motion, extending from crest to base of each ridge. Averaging was done parallel to this direction, rather than perpendicular to the ridge trend or thrust fault strike, because slip on these faults is locally oblique (Mugnier et al., 1999). Study areas and the exact regions from which profiles were extracted are shown in Figure DR1. Averaging in the direction of hanging-wall motion yielded approximately strike-wise topographic swath profiles where lows and highs represent transverse valleys and ridges, respectively (Fig. DR2). Wind gaps and peaks are evident in the ridge-line profile and commonly correspond spatially with valleys and ridges on the proximal and distal ridge flanks. For better comparison against model results (e.g., the null hypothesis simulation cross-correlation results in Fig. DR3), profiles were smoothed with a 500 m-wide moving averaging window.

Topographic profiles from the two opposing ridge flanks were then cross-correlated without a lag across the principal drainage divide, yielding a Pearson product-moment correlation coefficient, r (Davis, 1973; Borradaile, 2003).

Range width and drainage divide position depend on parameters N_e and α. Because simulated steady-state topography is sensitive to initial conditions and strict comparisons of correlation coefficient among individual simulations with different input

parameters is not meaningful, we used a Monte Carlo approach to constrain model

uncertainty and therefore better assess comparisons among model results (Borradaile,

2003). For each set of parameters, multiple realizations of each model (n = 10–200

depending on computational cost) were created using different horizontal initial surfaces

of randomly perturbed node elevations. In our study, we intended not to determine if a

given correlation coefficient was significant such as by using a t-test (Davis, 1973), but

rather to determine if the correlation coefficient associated with certain model parameters

was significantly different from the null hypothesis (i.e., r for simulations with no

horizontal bedrock motion).

APPENDIX DR2. Model description

Bedrock streamlines are controlled in the landscape evolution model by simple kinematic rules following Suppe (1983). Rock streamlines parallel the fault everywhere and bedrock has a velocity of V. This rate is equivalent to the fault-slip rate. Velocities change direction, but not magnitude, across axial surfaces. The dips of the detachments or flats are 0°; α is ramp dip and β is the axial surface dip, where $\beta = (180-\alpha))/2$. Above the fault ramp, the horizontal component, v, is defined as

$$v = V \cos \alpha \tag{A1}$$

The vertical component, u, is defined as

$$u = V \sin \alpha \tag{A2}$$

Note that this notation goes against the convention in physics where u is the x-directed velocity but conforms with common geologic usage where u is uplift rate.

The rate of fluvial erosion in bedrock channels is assumed to be proportional to unit stream power (Howard et al., 1994). Erosion rate, E, has units of m·yr^{-1} and is defined as

$$E = k_b \frac{Q}{W} S \tag{A3}$$

where k_b is the intrinsic erodibility (m^{-1}), Q is total water discharge (m^3·yr^{-1}), W is stream width (m), and S is stream slope (unitless).

We rewrite the stream power law in terms of upstream drainage area in order to allow simpler comparison with sites where area is readily measurable from DEMs but Q is not. Hydrologic and hydraulic variables are taken to be time-averaged quantities such that they can be more simply related to area.

First, we solve for Q using a simple relation for conservation of mass,

$$Q = PA \tag{A4}$$

where P is a spatially and temporally constant precipitation rate (m·yr^{-1}) and A is upstream drainage area (m^2). This relation also assumes there is no effective subsurface water storage or input and no evapotranspiration.

Second, we use an empirical relation for hydraulic geometry,

$$W = k_w Q^b \tag{A5}$$

where $b \approx 0.5$. This equation has been found to be an appropriate relation for both alluvial and bedrock streams (Leopold and Maddock, 1953; Montgomery and Gran, 2001; Whipple, 2004).

Combining equations (A3), (A4), and (A5), fluvial erosion rate is recast as

$$E = KA^m S^n \tag{A6}$$

where $K = \dfrac{k_b P^{\frac{1}{2}}}{k_w}$, $m = 1/2$, and $n = 1$.

Hillslope erosion is simulated with an equation for linear diffusion in two horizontal dimensions (Culling, 1965):

$$E = -\kappa\left(\frac{\partial^2 h}{\partial x^2} + \frac{\partial^2 h}{\partial y^2}\right) \tag{A7}$$

where κ is a spatially constant diffusivity ($m^2 \cdot yr^{-1}$).

Combining equations (A6) and (A7) and a tectonic velocity field in a continuity equation for landscape evolution yields:

$$\frac{\partial h}{\partial t} = u + v\frac{\partial h}{\partial x} + \kappa\left(\frac{\partial^2 h}{\partial x^2} + \frac{\partial^2 h}{\partial y^2}\right) - KA^{\frac{1}{2}}S \tag{A8}$$

To further simplify analysis, we nondimensionalize equation (A8):

$$\frac{\partial h*}{\partial t*} = u* + v*\frac{\partial h*}{\partial x*} + \frac{\kappa}{TV}\left(\frac{\partial^2 h*}{\partial x*^2} + \frac{\partial^2 h*}{\partial y*^2}\right) - \frac{KT}{V}A*^{\frac{1}{2}}S \tag{A9}$$

which is further simplified as

$$\frac{\partial h*}{\partial t*} = \sin\alpha + \cos\alpha\frac{\partial h*}{\partial x*} + D\left(\frac{\partial^2 h*}{\partial x*^2} + \frac{\partial^2 h*}{\partial y*^2}\right) - N_e A*^{\frac{1}{2}}S \tag{A10}$$

Definitions of the nondimensional variables and parameters are given in Appendix DR3.

In our model, the average nondimensional horizontal node spacing is 0.5, simulation space is 8 units long in the y-direction and its width varies as a function of N_e and D. All four model boundaries are open, except in model 1f, in which case the lateral boundaries are reflected. In contrast to all of the other simulations, which use the landscape evolution model CHILD (Tucker et al., 2001), for model 1f we use the landscape evolution model GOLEM, which is based on a regular grid (Tucker and Slingerland, 1994).

APPENDIX DR3. Equations for nondimensional variables and parameters

Spatial variables: $x^* = \dfrac{x}{T}$, $y^* = \dfrac{y}{T}$, $h^* = \dfrac{h}{T}$, $A^* = \dfrac{A}{T^2}$

Velocity: $u^* = \dfrac{u}{V}$, $v^* = \dfrac{v}{V}$

Time: $t^* = \dfrac{tV}{T}$

Erosional parameters: $D = \dfrac{\kappa}{TV}$, $N_e = \dfrac{KT^{2m}}{V}$

Relief: $R_v^* = \dfrac{R_v}{R_v^0}$, $R_w^* = \dfrac{R_w}{R_w^0}$

Flux: $\phi^* = v^* \cdot R_w^* = \cos\alpha \cdot R_w^*$

APPENDIX DR4. Estimation of erosion number in Siwalik Hills

Fluvial erosion number, N_e, was estimated for the Siwalik Hills using available constraints on its component parameters and constants (K, T, V, and m). In the region of study in the Siwalik Hills, hanging wall velocity ranges from 4–21 mm/yr based on the records of deformed Holocene river terraces above the Main Frontal Thrust and Main Dun Thrust (Lavé and Avouac, 2000; Mugnier et al., 2004). Hanging-wall thickness ranges from ~4–6 km (Mugnier et al., 1999; Lavé and Avouac, 2000). In the eastern region, near the Bakeya and Bagmati Rivers, estimates of K fall in the range 1.47×10^{-4}– 1.64×10^{-4} m$^{0.08}$/yr when $m = 0.46$ (Kirby and Whipple, 2001). Mean annual precipitation varies substantially across southern Nepal by a factor of ~4, indicating that the above value of K should also vary spatially, ignoring other factors such as lithology (Bookhagen et al., 2005). The eastern study area lies in a region of high precipitation rates relative to much of southern Nepal. Given that K scales with precipitation rate to a power of ~1/2 following the simplified formulation in Appendix DR2 (for a more complete derivation and formulation, see Whipple and Tucker, 1999), we might expect that K should vary due to precipitation by a factor of ~2. Bearing in mind that V and K are probably the least well-constrained parameters among our three sites, N_e likely falls between approximately 5 and 125.

APPENDIX DR5. Notation

x, y horizontal dimensions, m

h elevation of land surface, m

t time, yr

v horizontal component of bedrock velocity, m yr^{-1}

u vertical component of bedrock velocity, m yr^{-1}

A drainage area, m^2

Q water discharge, m^3 yr^{-1}

W stream width, m

S stream channel gradient, unitless

m area exponent in the stream-power erosion equation

T thickness of hanging wall, m

V bedrock velocity or slip rate above fault, m yr^{-1}

α ramp dip, °

β axial surface dip, °

κ diffusivity, m^2 yr^{-1}

k_b intrinsic bedrock incision coefficient, m^{-1}

k_w channel width coefficient, yr$^{1/2}$ m$^{-1/2}$

b channel width exponent, unitless

K stream power coefficient, yr^{-1}

D diffusion number, unitless

N_e erosion number, unitless

r Pearson product-moment correlation coefficient, unitless

R_w mean wind-gap relief, m

R_v mean cross-valley relief, m

R_w^0 mean wind-gap relief formed when ramp dip is 90°, m

R_v^0 mean cross-valley relief formed when ramp dip is 90°. m

$R_w{*}$ nondimensional wind-gap relief, unitless

$R_v{*}$ nondimensional cross-valley relief, unitless

$\phi{*}$ nondimensional lateral advection rate of relief across a ridge crest, unitless

TABLE DR1. CROSS-CORRELATION RESULTS FROM THE SIWALIK HILLS, NEPAL

Location	Coordinates		Convergence azimuth	α $(°)^{\dagger}$	T $(km)^{\dagger}$	$r^{\S}$	Length (km)	Maximum width	
	Lat. (°N)	Long. (°E)	(°)					South (km)	North (km)
Eastern									
A	27°15'	85°7'	~195	45	6	0.67	7.7	5	6
B	27°15'	85°12'	~195	40	5	0.89	5.0	3	5
C	27°12'	85°18'	~195	35	5	-0.02	4.7	4	5
D	27°11'	85°25'	~195	30	5	0.74	10.8	4	6
E	27°9'	85°35'	~195	30	5	0.26	13.0	4	5
Central									
F	27°50'	82°20'	~205	40	6	0.23	25.5	5	8
G	27°45'	82°45'	~205	40	5	0.13	22.5	7	4
Western									
H	28°45'	81°10'	~207	40	4	0.55	10.1	5	8
I	28°30'	81°35'	~207	35	4	-0.18	46.4	4	7
J	28°20'	81°35'	~207	30	4	0.30	33.6	4	4
Mean						$0.36 \pm 0.22^{\#}$			

[†] Based on Lavé and Avouac (2000) and Mugnier et al. (1999).
[§] Pearson product-moment correlation coefficient (r) is calculated from paired vectors of mean elevations of opposing, whole ridge flanks.
[#] The distribution of r passes the Lilliefors goodness-of-fit test for a normal distribution (5% significance level). The reported confidence interval is 95%.

TABLE DR2. LIST OF MODEL PARAMETERS AND CROSS-CORRELATION RESULTS

Model code	N_e	D	α (°)	T (km)	$r^{\dagger}$ mean	95% confidence interval	n
Vertical uplift simulations							
1a (*null hypothesis*)	10	0	90	10.0	0.118	0.027	200
1b	10	0	90	15.0	0.149	0.031	200
1c	10	0	90	20.0	$0.090^{\S}$	0.033	200
1d	100	0	90	10.0	0.148	0.027	200
1e	10	10^{-1}	90	10.0	0.121	0.031	200
1f[#]	10	0	90	10.0	0.118	0.041	100
Fault-bend fold simulations							
2a	2	0	30	5.0	0.547	0.073	10
2b	3	0	30	5.0	0.509	0.073	10
2c	5	0	30	5.0	0.338	0.070	10
2d	10	0	30	5.0	0.229	0.126	10
2e	15	0	30	5.0	0.134	0.111	10
2f	50	0	30	5.0	0.192	0.105	10
2g	100	0	30	5.0	0.117	0.105	10
3a	10	10^{-5}	30	5.0	0.230	0.121	10
3b	10	10^{-4}	30	5.0	0.224	0.127	10
3c	10	10^{-3}	30	5.0	0.207	0.107	10
3d	10	10^{-2}	30	5.0	0.262	0.135	10
3e	10	10^{-1}	30	5.0	0.280	0.108	10
3f	10	10^{0}	30	5.0	0.324	0.108	10
3g	10	10^{1}	30	5.0	0.524	0.046	10
4a	10	0	10	1.7	0.042	0.102	10
4b	10	0	20	3.4	0.150	0.068	10
4c	10	0	30	5.0	0.195	0.077	10
4d	10	0	40	6.4	0.182	0.087	10
4e	10	0	50	7.7	0.193	0.105	10
4f	10	0	60	8.7	0.122	0.100	10
4g	10	0	70	9.4	0.089	0.103	10
4h	10	0	80	9.9	0.020	0.109	10
5a	5	0	10	1.7	0.191	0.141	10
5b	5	0	20	3.4	0.267	0.057	10
5c	5	0	30	5.0	0.299	0.104	10
5d	5	0	40	6.4	0.360	0.120	10
5e	5	0	50	7.7	0.294	0.099	10
5f	5	0	60	8.7	0.252	0.124	10
5g	5	0	70	9.4	0.258	0.114	10
5h	5	0	80	9.9	0.099	0.086	10

[†] Correlation coefficient is calculated for mean elevations of entire ridge flanks.

[§] The distribution is not normal as determined by the Lilliefors test at the 5% significance level. The p-value of this individual test is 0.035.

[#] Model 1f differs from 1a in that 1a has lateral boundaries at fixed elevations and model 1f has reflected boundaries, which wrap around and are continuous with the opposite edge. In contrast to all other model runs, this was conducted using the landscape evolution model GOLEM, which is based on a regular grid (Tucker and Slingerland, 1994).

REFERENCES CITED

Bookhagen, B., Thiede, R.C., and Strecker, M.R., 2005, Abnormal monsoon years and their control on erosion and sediment flux in the high, arid Northwest Himalaya: Earth and Planetary Science Letters, v. 231, p. 131-146.

Borradaile, G., 2003, Statistics of Earth Science Data: Berlin, Springer-Verlag, 351 p.

Culling, W.E.H., 1965, Theory of erosion on soil-covered slopes: Journal of Geology, v. 73, p. 230-254.

Davis, J.C., 1973, Statistics and Data Analysis in Geology: New York, John Wiley and Sons, 550 p.

Howard, A.D., Dietrich, W.E., and Seidl, M.A., 1994, Modeling fluvial erosion on regional to continental scales: Journal of Geophysical Research, v. 99, p. 13,971-13,986.

Kirby, E., and Whipple, K., 2001, Quantifying differential rock-uplift rates via stream profile analysis: Geology, v. 29, p. 415-418.

Lavé, J., and Avouac, J.P., 2000, Active folding of fluvial terraces across the Siwaliks Hills, Himalayas of central Nepal: Journal of Geophysical Research, v. 105, p. 5735-5770.

Leopold, L.B., and Maddock, T., Jr., 1953, The hydraulic geometry of stream channels and physiographic implications: U. S. Geological Survey Professional Paper 252, p. 57.

Montgomery, D.R., and Gran, K.B., 2001, Downstream variations in the width of bedrock channels: Water Resources Research, v. 37, p. 1841-1846.

Mugnier, J.-L., Huyghe, P., Leturmy, P., and Jouanne, F., 2004, Episodicity and rates of thrust-sheet motion in the Himalayas (western Nepal), *in* McClay, K.R., ed., AAPG Memoir, v. 82, p. 91-114.

Mugnier, J.L., Leturmy, P., Mascle, G., Huyghe, P., Husson, L., Chalaron, E., Vidal, G., and Delcaillau, B., 1999, The Siwaliks of western Nepal; I, Geometry and kinematics: Journal of Asian Earth Sciences, v. 17, p. 629-642.

Suppe, J., 1983, Geometry and kinematics of fault-bend folding: American Journal of Science, v. 283, p. 684-721.

Tucker, G.E., Lancaster, S.T., Gasparini, N.M., Bras, R.L., and Rybarczyk, S.M., 2001, An object-oriented framework for distributed hydrologic and geomorphic modeling using triangulated irregular networks: Computers & Geosciences, v. 27, p. 959-973.

Tucker, G.E., and Slingerland, R.L., 1994, Erosional dynamics, flexural isostasy, and long-lived escarpments; a numerical modeling study: Journal of Geophysical Research, v. 99, p. 12,229-12,243.

Whipple, K.X., 2004, Bedrock rivers and the geomorphology of active orogens: Annual Review of Earth and Planetary Sciences, v. 32, p. 151-185.

Whipple, K.X., and Tucker, G.E., 1999, Dynamics of the stream-power river incision model; implications for height limits of mountain ranges, landscape response timescales, and research needs: Journal of Geophysical Research, v. 104, p. 17,661-17,674.
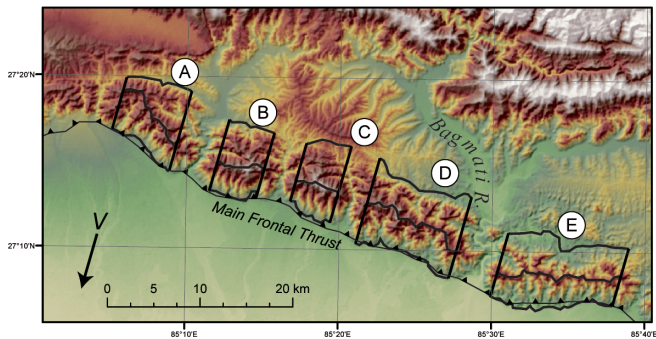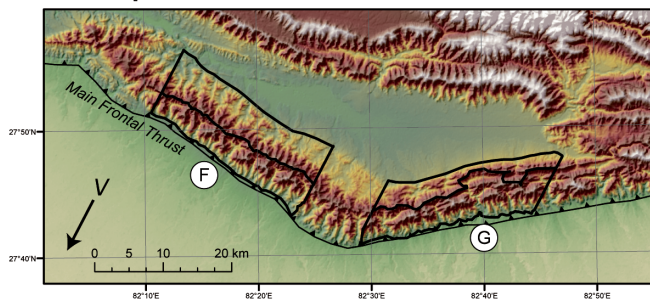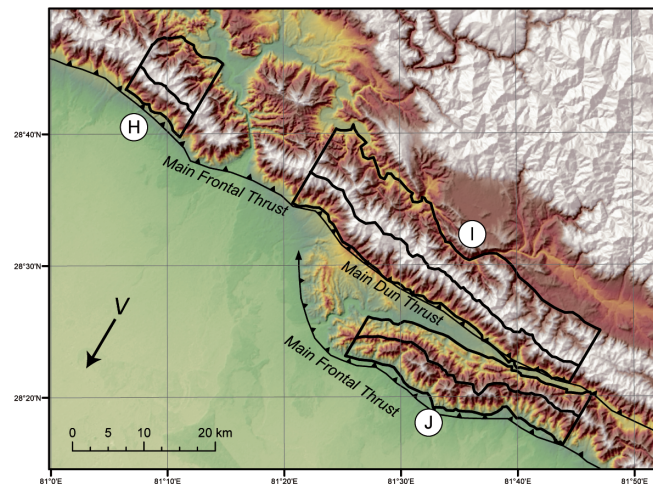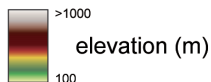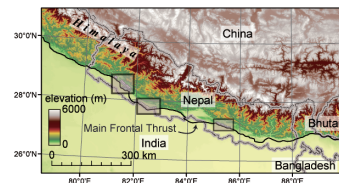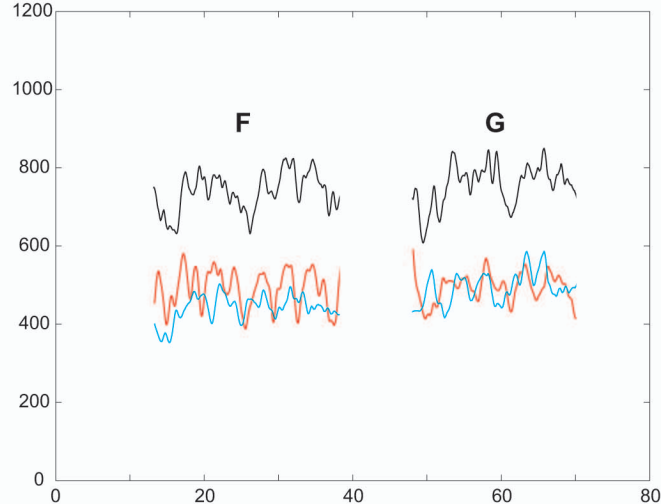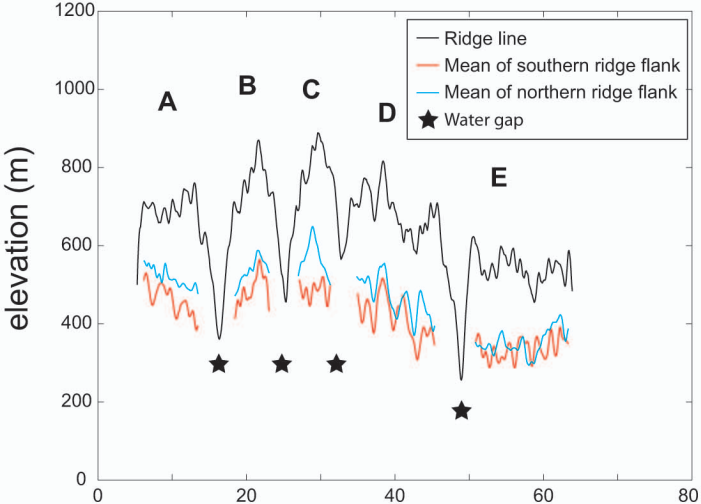
Figure DR1. Shaded relief maps from eastern, central, and western Nepal showing locations along the Siwalik Hills that were used in topographic cross-correlations, marked with black polygons. Location map is at bottom right with black boxes representing the three regions. Direction of hanging wall transport (or convergence) is shown with an arrow labeled *V*.
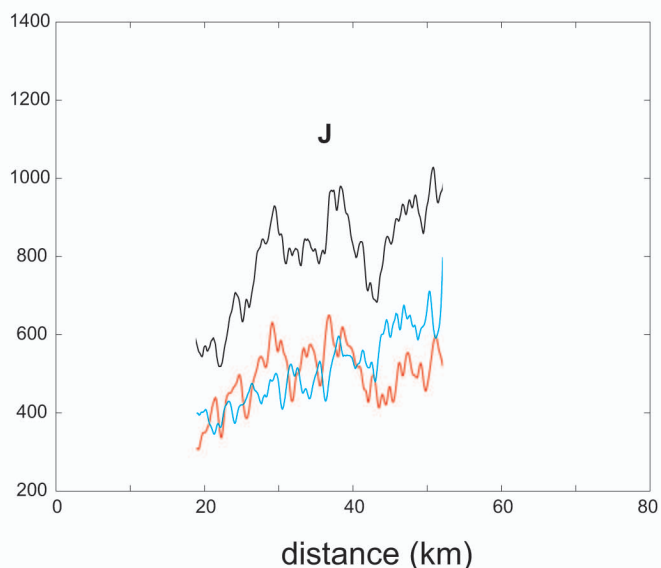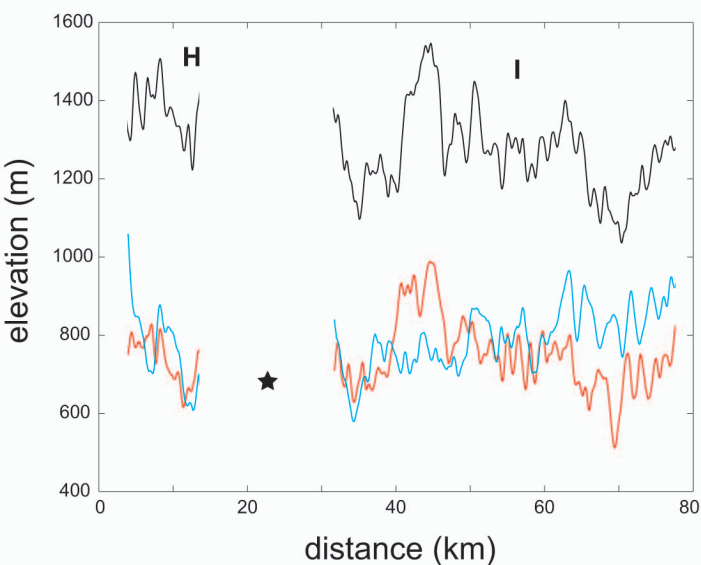
Figure DR2. Elevation profiles measured perpendicular to the convergence direction of the hanging wall. Ridge profiles are shown in black. Profiles in red and blue represent the mean elevations of the southern (red) and northern (blue) flanks of the ridge. Breaks in profiles are located at water gaps and bends in the ridge. Profiles have been smoothed with a 500-m wide moving window to reduce local topographic noise (produces topographic roughness comparable to the model with a 500 m node spacing). Locations of these profiles are shown in Figure DR1.
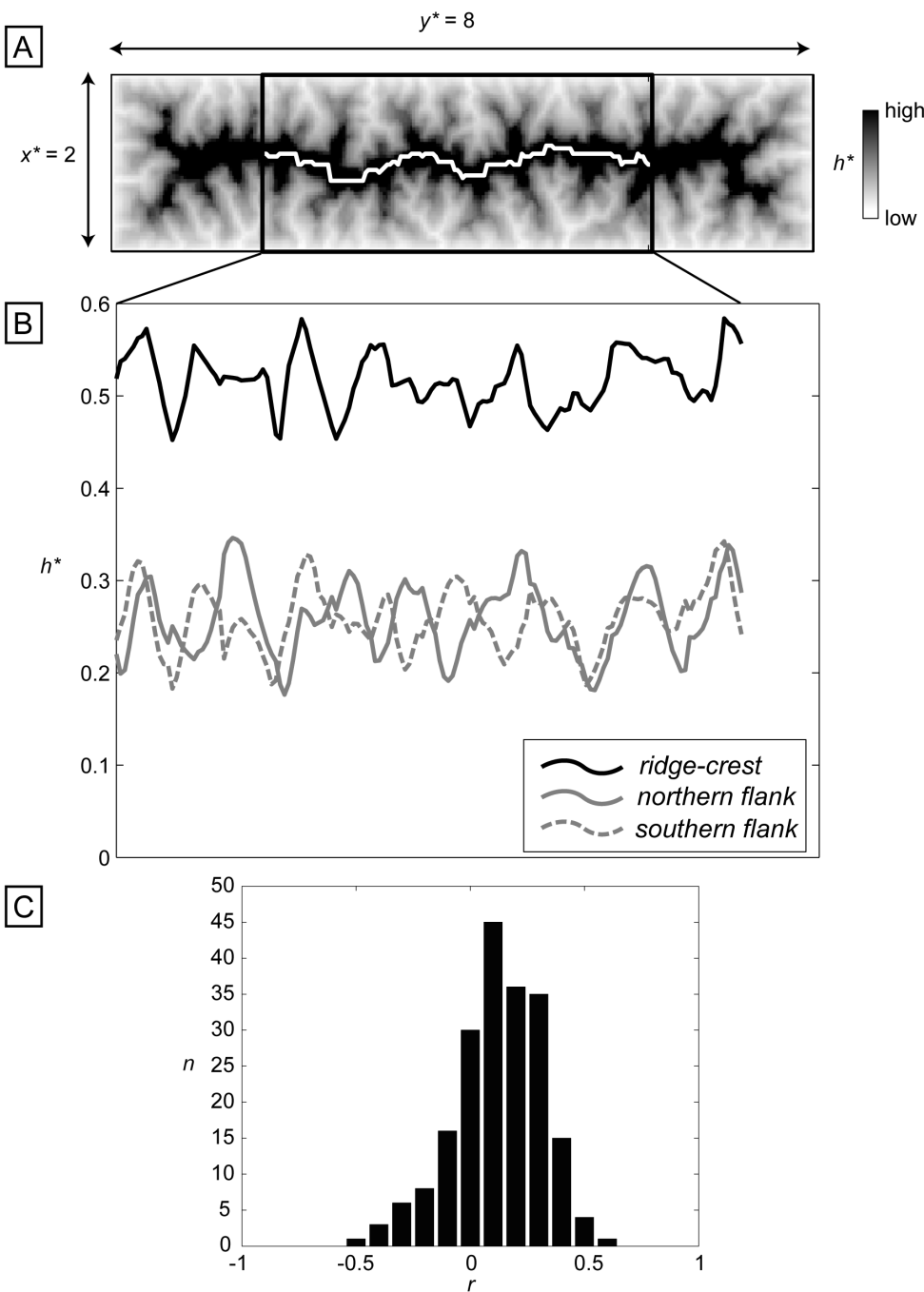
Figure DR3. Results of the vertical rock uplift model (model 1a). (A) Elevation map, in which darker shades indicate higher elevations. Ridge line is marked in white. (B) Topographic profiles of the ridge line and mean elevations from the "southern" and "northern" flanks of the ridge, in which elevations are averaged along columns. (C) Histogram of r from 200 realizations of model 1a.